Supplement of Atmos. Chem. Phys., 21, 635–655, 2021
https://doi.org/10.5194/acp-21-635-2021-supplement

Atmospheric Chemistry and Physics
Open Access

Supplement of

Variability in the mass absorption cross section of black carbon (BC) aerosols is driven by BC internal mixing state at a central European background site (Melpitz, Germany) in winter

Jinfeng Yuan et al.

Correspondence to: Robin Lewis Modini (robin.modini@psi.ch)

Supplement

Table S1. Characteristics of the campaign Periods (median and IQR)

periods parameters	period 1 (02. Feb 09:00 - 05. Feb 21:00)	period 2 (05. Feb 21:00 - 14. Feb 22:00)	period 3 (14. Feb 22:00 - 23. Feb 00:00)	short plume (18. Feb 17:00 - 19. Feb 07:00)
Dominant air mass origin	S to SW	NE to SE	W	NW
Local wind speed (m/s)	1.2 (0.8–1.7)	3.4 (2.7–4.1)	4 (2.5–6.3)	1.5 (1.2–1.7)
Gas ratio of SO_2 to NO_X	0.08 (0.04– 0.11)	0.63 (0.28– 0.83)	0.12 (0.09– 0.19)	0.09 (0.08– 0.09)
$D_{\mathrm{modal\_rBC}}$ (nm)	190 (183–193)	239 (232–242)	181 (169–199)	242 (192–298)
Total aerosol concentration ($\mu g\ m^{-3}$)	10.6 (8.7–11.7)	23.0 (20.4–27.2)	10.9 (8.1–15.8)	8.1 (6.6–10.2)
Mass fractions of organics (%)	36 (35–38)	37 (33–39)	29 (23–35)	28 (25–31)
Mass fractions of BC (%)	12 (10–16)	14 (12–15)	7 (4–11)	14 (9–21)
Mass fractions of nitrate (%)	24 (20–28)	18 (17–20)	35 (25–41)	27 (25–30)
Mass fractions of sulfate (%)	13 (11–17)	19 (17–22)	12 (11–15)	11 (10–12)

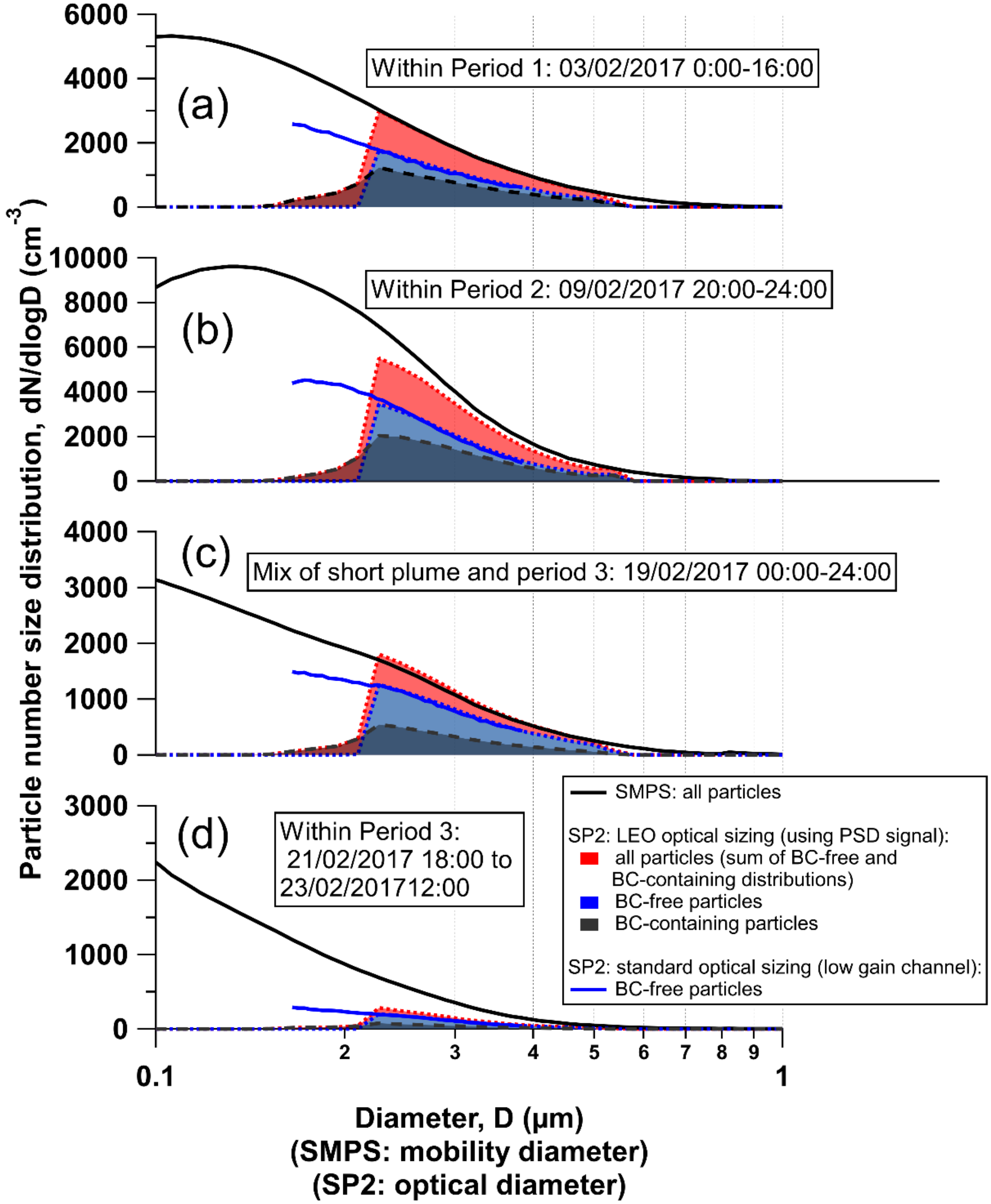

Figure S1. Cross check of total particle number size distribution measured by SP2 compared with that from SMPS.

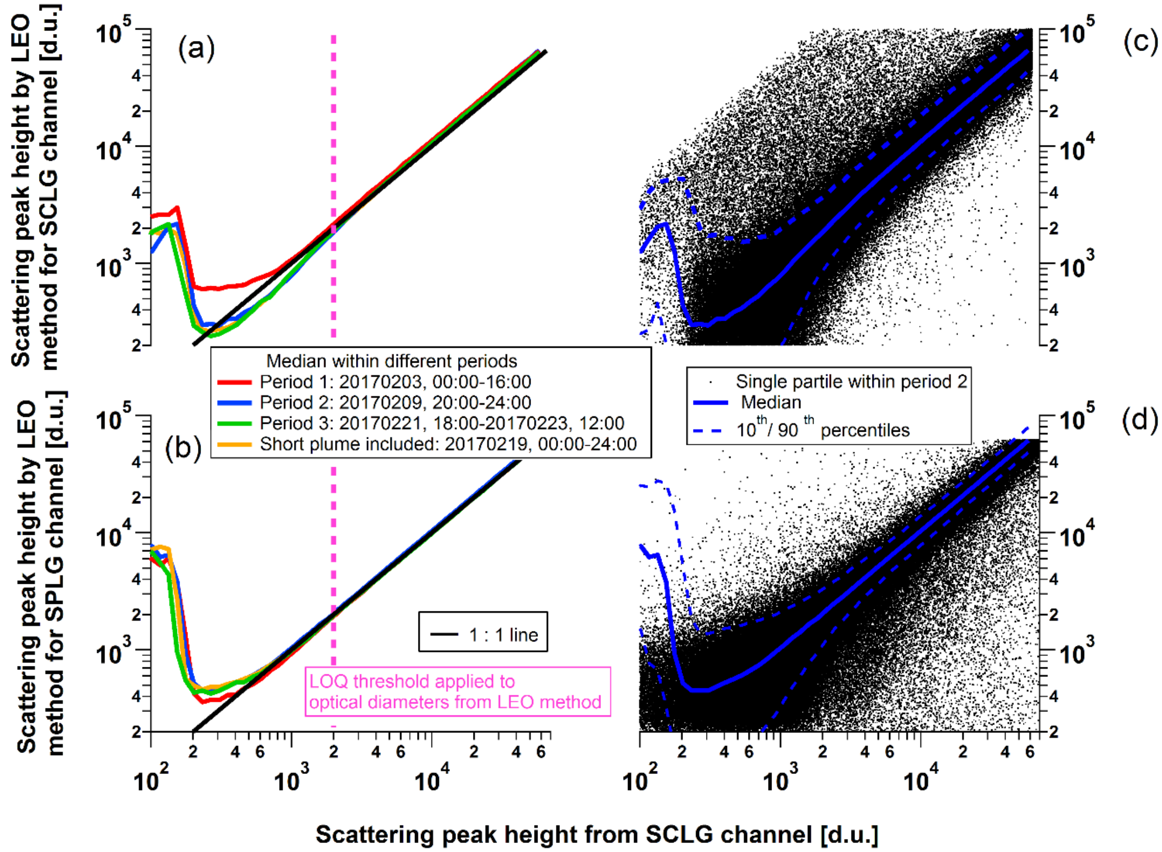

Figure S2. Verification of LEO method by BC-free particles. (a) Median of LEO scattering peak height vs standard scattering peak height from low gain scattering detector (SCLG) for four example days during different periods of the campaign. Scaling factors were applied to correct minor bias in the LEO fit analysis, i.e. to make the LEO fit results match the standard peak analysis. (b) LEO scattering peak height retrieved from the low gain position sensitive detector (SPLG) vs standard scattering peak height from the low gain scattering channel. (Adjustable scaling factors were applied to tie the LEO-fit to the calibration of the low gain scattering channel. (c) and (d) show single particle data corresponding to (a) and (b), respectively.

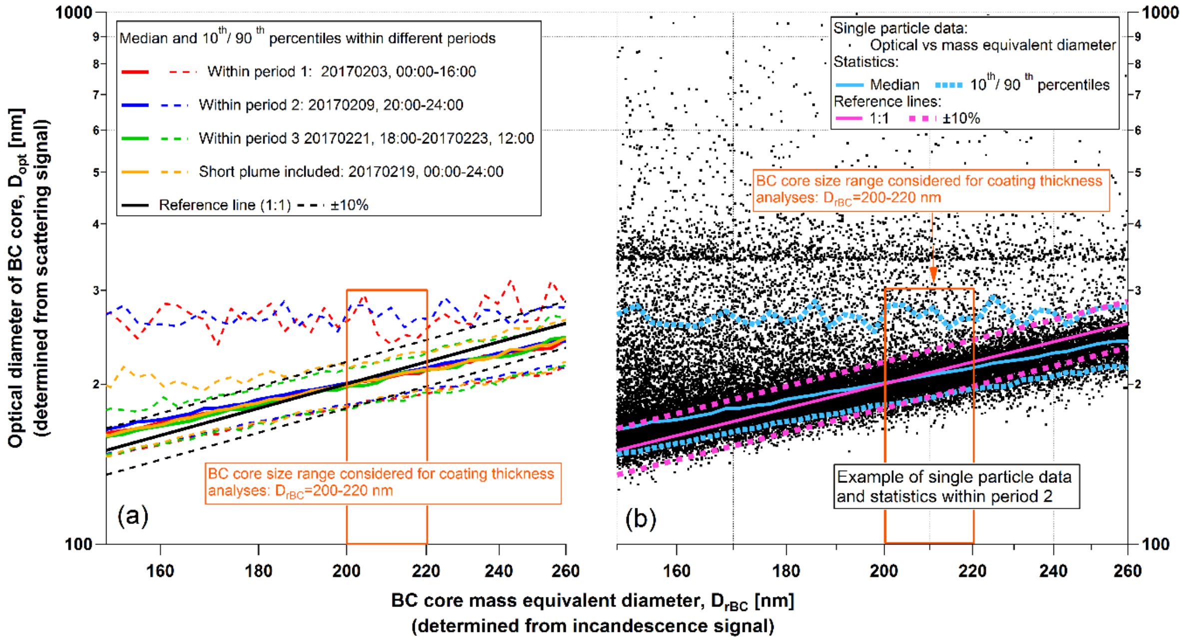

Figure S3. Verification of LEO fit: Optical diameter of the bare BC core compared with the rBC mass equivalent diameter. (a) Median and 10th and 90th percentiles of the single particle data. (b) Single particle data and corresponding statistics for period 2 as an example. The LEO fit results were used for the BC core diameter range from 200 nm to 220 nm, in which uncoated and coated particles can be sized optically. Within this size range the median values fall on the1 to 1 line within 2 %. This ensures accuracy of the reported coating thickness for bare BC particles, i.e. that particle reported to have a coating thickness of zero indeed represent uncoated BC, except for the random noise present on single particle level.

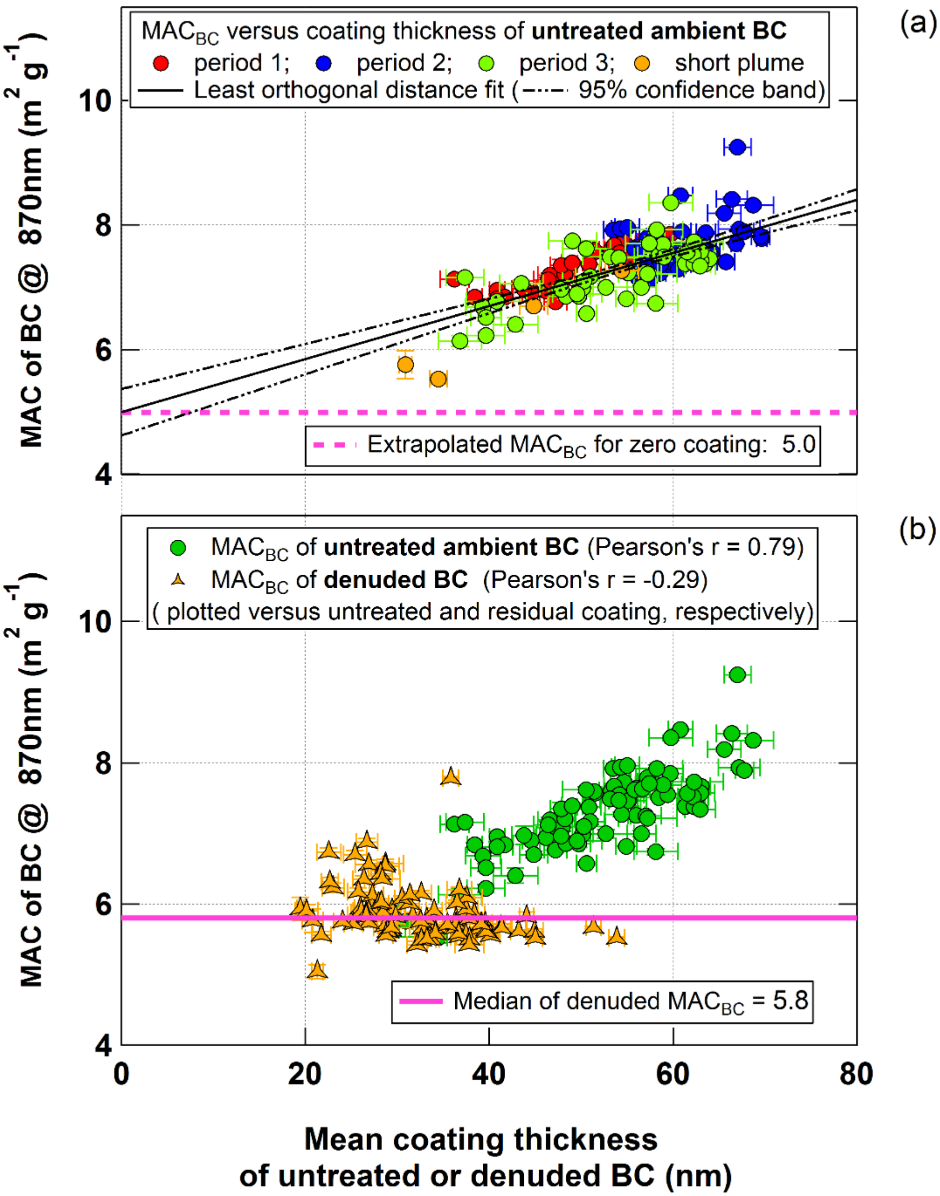

Figure S4. Repeated version of Fig. 6 in the main text with one change made: in panel b) the denuded MAC$_{BC}$ values are plotted against the coating thickness of the denuded particles, rather than the coating thickness of the untreated particles as in Fig. 6.

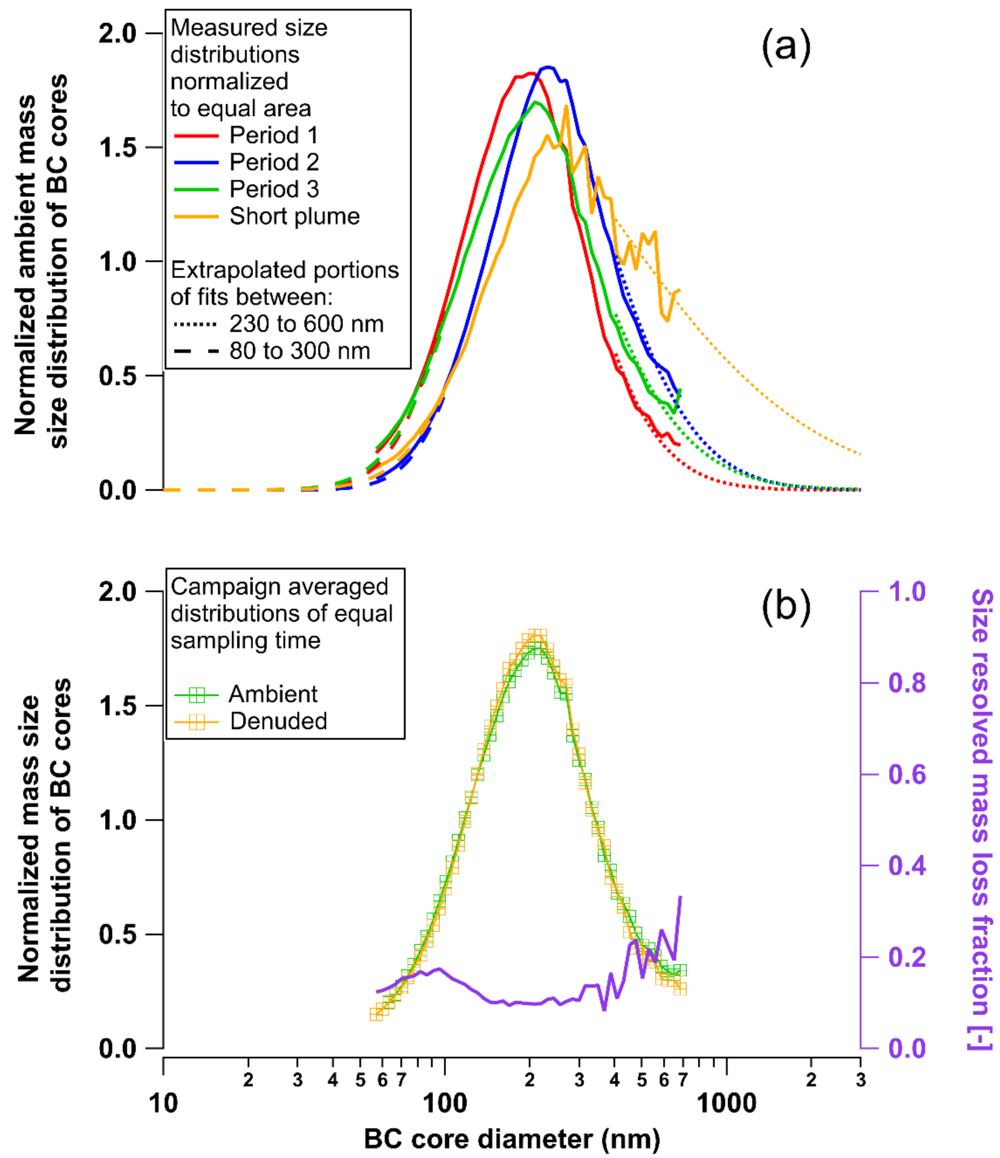

Figure S5. Normalized rBC mass size distributions as a function of BC core mass equivalent diameter. Average distributions measured during ambient conditions for each of the different campaign periods are shown in (a), and ambient and denuded distributions averaged over the full campaign period (with equal sampling times) are shown in (b). The size resolved mass loss fraction within the catalytic stripper, computed from the denuded and ambient size distributions, is also shown in (b). Panel (a) displays the extrapolated

portions of two different types of lognormal fits that were applied to the measured distributions for each period in order to estimate the missing BC mass beyond the lower and upper SP2 detection limits.

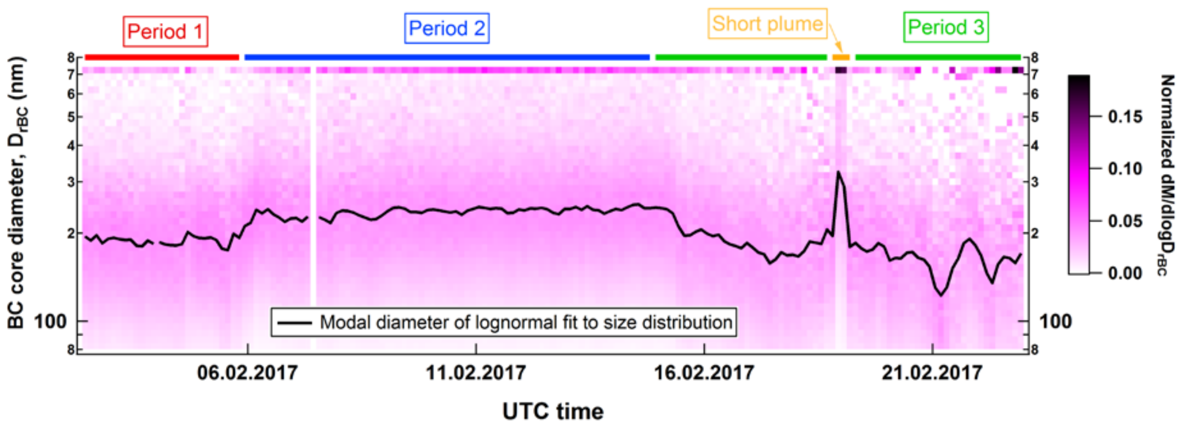

Figure S6. Time series of the normalized ambient rBC mass size distribution (at 3 h time resolution) as a function of BC core mass equivalent diameter (D_{rBC}). The overflow size bin including all BC particles D_{rBC} greater than ~700 nm is also shown.

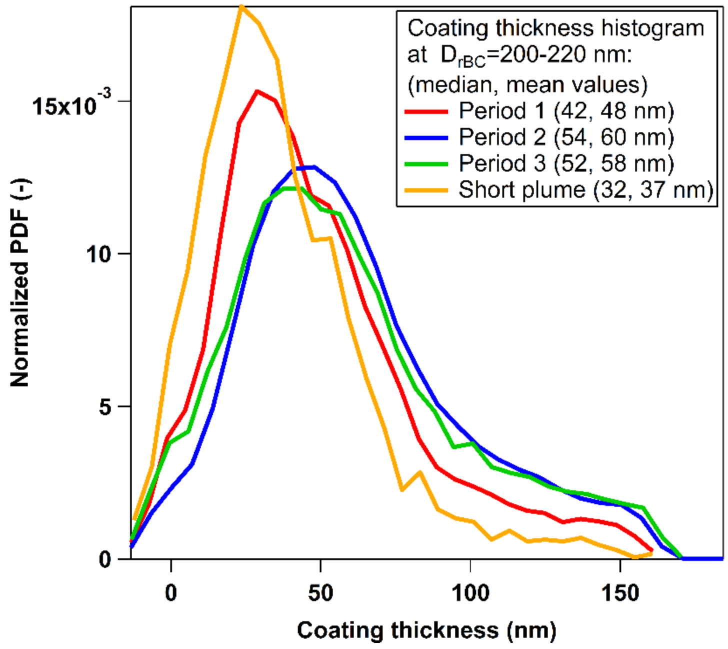

Figure S7. Histograms of BC particle coating thickness on single particle level separately shown for the three periods and the short plume.

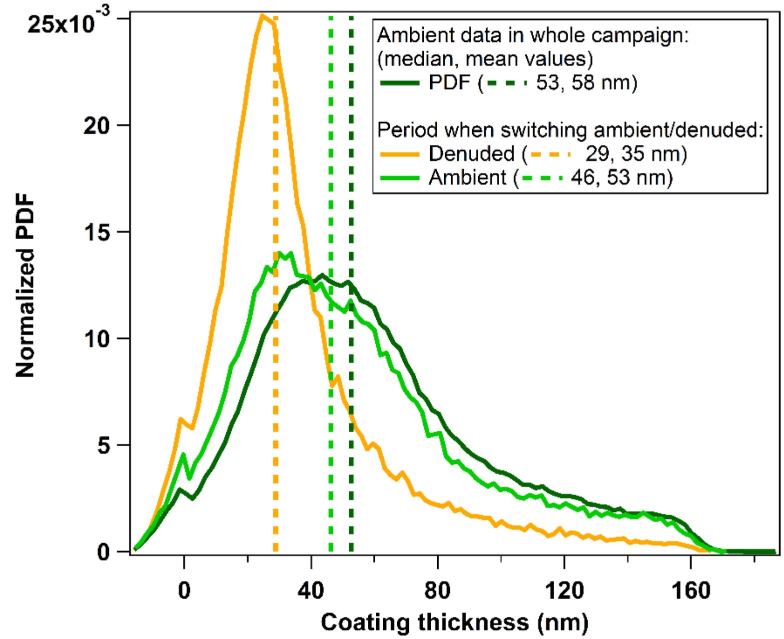

Figure S8. Histograms of BC particle coating thickness on single particle level for rBC mass equivalent core diameters between 200 nm to 220 nm. Histograms are separately shown for the whole campaign (ambient sample only) and for the period when the denuder was operated (ambient and denuded samples).

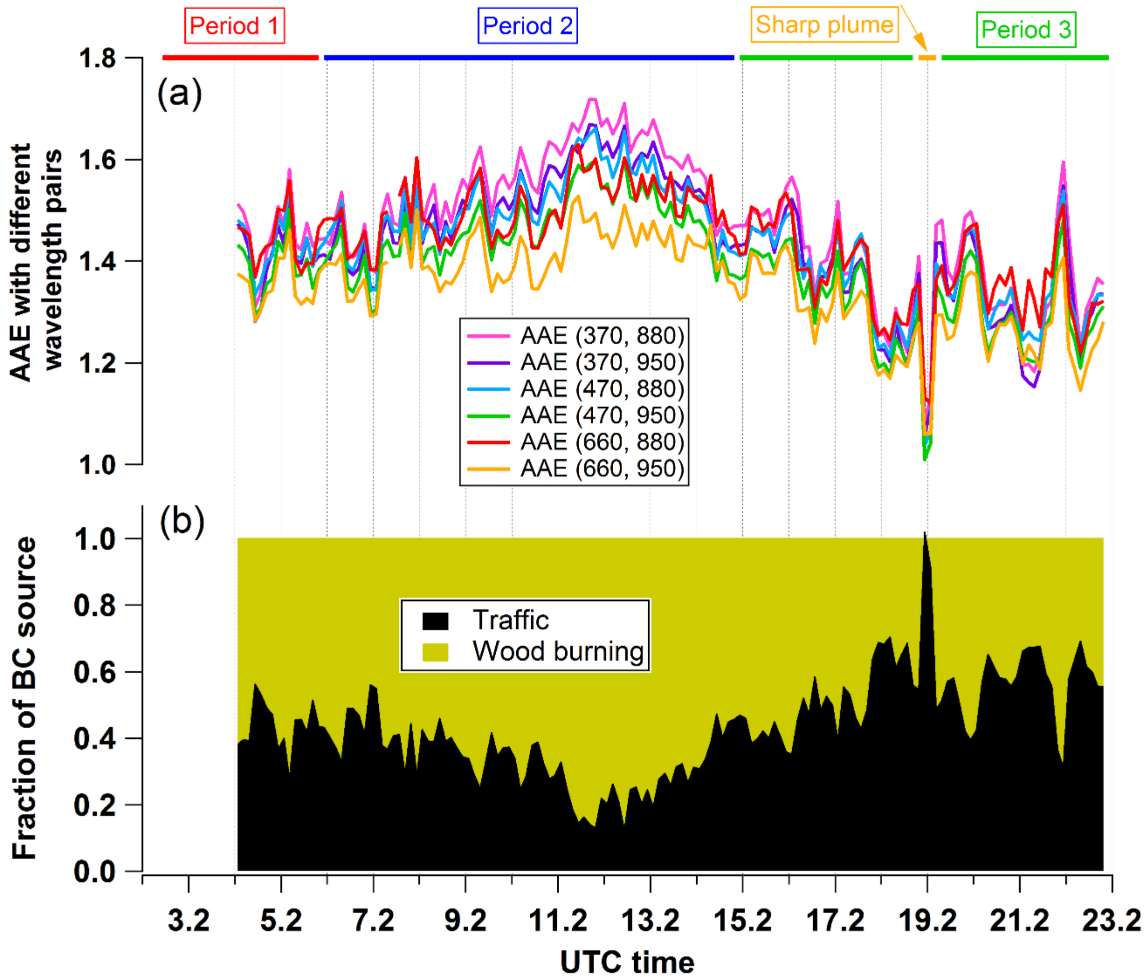

Figure S9. (a) Time series at 3 h time resolution of AAE of different pairs of wavelengths, and (b) the estimated fractional contribution of traffic and wood burning emissions to BC mass. The attribution of sources was done using the so-called "aethalometer model" using the coefficients reported in Zotter et al. (2017). Note that traffic and wood burning fractions are upper limits as BC from coal burning, which is potentially present, could be assigned to either source.

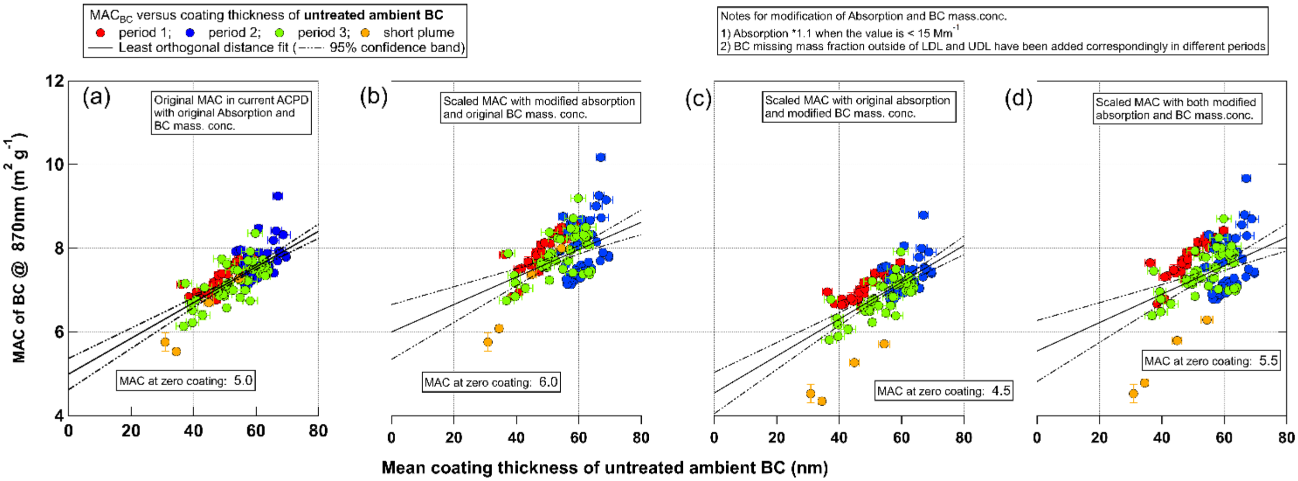

Figure S10. Panel a) is a repeated version of Fig. 6a in the main text. Panel b) displays the same quantities but with an additional correction factor of 1.1 applied to the MAC of BC values corresponding to absorption coefficients less than 15 Mm^{-1} (as motivated by Fig. 2 and the discussion in Sect. 2.4.2.2), panel c) displays the same quantities but with period-dependent missing mass correction factors applied to the MAC of BC values (as discussed in Sect. 2.4.1), and panel d) displays the same quantities but with both the loading-dependent absorption scaling factors and period-dependent missing mass correction factors applied to the MAC of BC values.